TRANSLATIONAL CHEMISTRY
AN INTERFACE JOURNAL
HTTPS://WWW.TRANSLATIONALCHEMISTRY.COM/

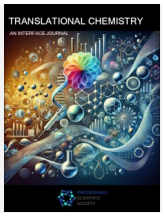

ORIGINAL ARTICLE | DOI: 10.5584/translationalchemistry.v1i2.248

Smartphone-based Colorimetric Protein Quantification in Human Urine Using Gold Nanoparticles

Beatriz Quintas[¥,1], Joana Galhano[¥,1], Hugo M. Santos[*,1,2], Elisabete Oliveira[*,1,2,3]

[1]BIOSCOPE Research Group, LAQV-REQUIMTE, Chemistry Department, NOVA School of Science and Technology, NOVA University of Lisbon, 2829-516, Caparica, Portugal. [2]PROTEOMASS Scientific Society, 2825-466, Costa de Caparica, Portugal. [3]Canterbury Christ Church University, School of Human and Life Sciences, Life, Sciences Industry, Liaison Lab, Sandwich, UK. [¥]Both authors contributed equally to this work.

Received: 25 November 2025 **Accepted:** 27 November 2025 **Available Online**: 5 December 2025

Abstract

Proteinuria, the presence of elevated protein levels in urine, is an important biomarker associated with various diseases. This study presents a portable, smartphone-based approach for colourimetric protein detection using gold nanoparticles (AuNPs). By inducing the aggregation of AuNPs in the presence of albumin, facilitated by sodium chloride, distinct colour changes were observed and quantified *via* smartphone image analysis. The method was tested using three smartphone models on urine samples from six volunteers, demonstrating a detection limit of 1.19 µg/mL and the ability to visually detect protein concentrations as low as 25 µg/mL. Furthermore, we successfully quantified the urinary proteome of a CRC patient, obtaining a protein concentration of 37 ± 3 µg/mL, which closely agrees with the value of 41 ± 1 µg/mL determined by the Bradford assay. This technique offers a rapid, cost-effective, and non-invasive tool for urinary protein detection, with promising applications in routine clinical diagnostics and disease monitoring.

Keywords: Protein quantification, Proteinuria, Colourimetric detection, RGB analysis, Smartphone-based analysis, Point-of-care testing.

1. Introduction

Proteinuria, characterised by elevated concentrations of protein in the urine, is often associated with an increased risk of renal failure [1,2], along with other health conditions like heart disease, diabetes, and infections [3]. Typically, healthy kidneys filter out less than 150 mg of protein daily, with approximately 20 mg of that being albumin [4]. Protein concentrations in urine ranging from 30 to 300 mg per day are classified as microalbuminuria, while those exceeding 300 mg per day are classified as proteinuria [3]. Additionally, if the daily concentration exceeds 3.5 g of protein, it is categorised as nephrotic range proteinuria. Proteinuria may arise from direct damage to the kidney's glomeruli or from the immune system's response to an infection occurring elsewhere in the body [5]. Frontline protein concentration evaluation in urine is often performed through a urine dipstick analysis. Although it does not require complex sample preparation before analysis as some other methods, it has low sensitivity for lower protein concentrations, for individuals with an albumin/creatinine ratio (ACR) ≥ 30 mg/g, being only recommended as a screening tool in older outpatients with ACR ≥ 300 mg/g [6]. As such, these dipsticks might prove inconclusive for some evaluations with a lower protein concentration.

Other methods can be used for a more accurate protein concentration determination, such as mass spectrometry, immunoassays, fluorescence spectroscopy or Raman spectroscopy. However, these require more extensive sample preparation protocols, are more labour-intensive and time-consuming, and also require expensive equipment [3]. Other colorimetric methods, such as the Bradford assay or the Bicinchoninic Acid (BCA) Assay, can also be used to estimate total protein concentration. However, all these have specific limitations, such as incompatibility with surfactants, a wide range of requirements on needed reagents, or lack of specificity for proteins [7]. Apart from these more conventional methods for protein detection, nanomaterials can also be used to detect protein in urine. Several studies in the literature report protein-nanoparticle interactions, often accompanied by colorimetric alterations and the occurrence of precipitation [8]. Moreover, the formation of a protein corona is also described when protein and nanoparticles dynamically interact with each other, forming hard and soft coronas. These interactions depend on many factors, namely, the surface functionalisation of the nanoparticles, nanoparticle surface charge and size, protein composition, and incubation time [9–12]. The adsorption of different proteins to form a protein corona *via* colorimetric changes was quantitatively

***Corresponding author:** Hugo M. Santos and Elisabete Oliveira (hmsantos@fct.unl.pt and ej.oliveira@fct.unl.pt)

characterised by UV-vis absorption spectroscopy [13]. In this assay, four models of proteins were successfully determined with a concentration range of up to 80 µg/mL in water and up to 200 µg/mL in human urine. Moreover, this assay also stands out from conventional commercial protein assays since it allows instantaneous quantification. However, despite being a faster and easier technique, absorption spectroscopy is still necessary for quantification. In recent years, there has been increasing interest in integrating smartphones and image processing programs into chemical analysis, facilitating environmentally friendly, rapid, and cost-effective analytical procedures [14]. Extensive research has been conducted on digital image colourimetry (DIC) as a versatile qualitative and quantitative analysis technique across various sample types, including heavy metals [15], pesticides [16], antibiotics [17], and food products [18]. Despite its versatility, DIC has been underutilised for protein quantification, leaving a significant gap in the research and application of this technique for protein analysis and detection of proteinuria.

Taking advantage of these points, our work sheds light on the development of a more accurate method. Gold nanoparticles (AuNPs) show distinct colours according to the protein-nanoparticle ratios. This allows for a visual determination of albumin in water and protein in urine samples with a minimum concentration of 25 µg/mL. To make the method accessible to everyone, a mathematical model was developed based on the Red-Green-Blue (RGB) characteristics of the colorimetric responses. This model enables the calculation of protein concentration from a simple smartphone image, providing a convenient, fast, and portable solution for protein quantification. As such, the use of nanotechnology combined with DIC methods for protein quantification could bring some advantages for preliminary screenings, not requiring extensive equipment and utilizing a simple sample preparation.

2. Materials and methods

2.1. Chemicals and Starting Materials

Hydrogen tetrachloroaurate (III) trihydrate (99.99%) was purchased from Thermo Scientific. Sodium citrate, tribasic dihydrate (≥ 99%), Bovine Serum Albumin (BSA ≥ 96%) and Bradford reagent were purchased from Sigma-Aldrich. Reagents were used as received.

2.2. Instrumentation

The Nanoparticle size and zeta potential were determined using a Dynamic Light Scattering (DLS) Malvern NanoZetasizer, with a 633 nm laser diode (PROTEOMASS Scientific Society, Caparica, Portugal). UV-Vis absorption spectra were acquired in a Jasco V-650 Spectrophotometer (Jasco Corporation, Tokyo, Japan). 96-well plate readings were performed using a CLARIOSTAR Spectrophotometer (BMG Labtech) (PROTEOMASS Scientific Society Facility). Transmission Electron Microscopy (TEM) images were obtained in a JEOL JEM-2100-HT operating at 200 kV; TEM images were collected using a "OneView" 4k×4k CCD camera. Photography of the 96-well plates for the RGB assessment assay was taken using smartphones, models OPPO Reno8 Lite, Samsung Galaxy S21 FE 5G and an iPhone 14 Pro. The Simplicity® UV ultrapure water purification system from Merck Millipore was used to produce ultrapure water for all the experiments.

2.3. Gold Nanoparticle Synthesis and Characterization

AuNPs were synthesised according to an already established Turkevich method [19]. Briefly, 4.9 mg of hydrogen tetrachloroaurate (III) was dissolved in 12.5 mL of ultrapure H_2O, and the obtained solution was heated at 100 ºC under stirring at 300 rpm. Then, 1.25 mL of a 10 mg/mL sodium citrate aqueous solution was added to the reactional mixture, and it was left under reflux for approximately 15 minutes until a deep red colour was observed. After the colorimetric alteration, the solution was left to cool down to room temperature. Until further use, the obtained nanoparticles were stored as obtained at 4 ºC to avoid degradation.
The obtained nanoparticles were promptly characterized by acquiring the respective absorption spectrum, and their size and zeta potential were determined through DLS measurements. TEM images were collected to evaluate particle size and morphology.

2.4. Albumin Colorimetric Detection with AuNPs in Aqueous Media

To analyse possible protein interactions with **AuNPs** the following experiments were conducted and measured by DLS and UV-Vis spectrum: **AuNPs** (1.7 mL H_2O + 300 µL AuNPs + 1.01 mL H_2O); **AuNPs-BSA** (1.7 mL H_2O + 300 µL AuNPs + 10 µL BSA 2 mg/mL + 1 mL H_2O); **AuNPs-BSA-NaCl** (1.7 mL H_2O + 300 µL AuNPs + 10 µL BSA 2 mg/mL + 1 mL NaCl 5 M); **AuNPs-NaCl** (1.7 mL H_2O + 300 µL AuNPs + 10 µL H_2O + 1 mL NaCl 5 M). To further evaluate the system's colorimetric behaviour, a high-throughput miniature set of experiments following similar conditions was performed in a 96-well plate. In a 96-well plate, a gradient concentration of BSA in aqueous solution, ranging from 0 to 97 µg/mL, was prepared with a total volume of 170 µL per well. Next, 30 µL of the synthesised AuNPs were added to each well. Finally, 20 µL of an aqueous 5 M NaCl solution was added to each well. Respective controls, without BSA and NaCl, were also performed under the same conditions.

2.5. Total Protein Colorimetric Detection with AuNPs in Urine Samples

2.5.1. *Urine sample collection and treatment*

Six urine samples from healthy volunteers and one from a colorectal cancer patient (CRC patient) were collected in sterile collection flasks following informed consent. Before handling, the urine was filtered through a paper filter to remove precipitates. The filtered urine was then diluted 1:20 using ultrapure H_2O and used throughout the study.

2.5.2. *Total Protein Colorimetric Detection with AuNPs in Urine Samples*

Healthy urine samples were spiked with varying concentrations of BSA (from a stock solution of 2 mg/mL) ranging from 0 to 97 µg/mL. In a 96-well plate, 170 µL of each spiked urine solution and CRC patient urine was added, followed by 30 µL of AuNPs and 20 µL of NaCl. One row of wells without NaCl was used as a negative control to evaluate the response without NaCl.

2.6. Protein Quantification

2.6.1. *Total Protein Quantification using Bradford Assay*

Total protein quantification of CRC patient urine was performed through a Bradford protein assay [20]. A calibration curve was generated using the following concentrations of BSA stock solutions in ultrapure H_2O: 0, 0.25, 0.5, 1.0 and 1.4 g/L. Five microliters of each stock solution were added to a 96-well plate, followed by 250 µL of the Bradford reagent. Five microliters of each urine sample were also added to the 96-well plate with 250 µL of the Bradford reagent. Each experiment was performed in duplicate. The UV-Vis measurements were conducted at 595 nm.

2.6.1. *Protein Quantification using the RGB Method*

A calibration curve was obtained by photographic collection of a BSA aqueous gradient in water from 0 to 97 µg/mL in the presence of AuNPs and NaCl in a transparent 96-well plate. Smartphone models used for photographic collection were Samsung Galaxy S21 FE 5G, OPPO Reno 8 Lite and iPhone 14 Pro. After photograph collection, an RGB analysis of each well was conducted with the image software ImageJ. Mean and specific channel values (red channel, green channel, and blue channel) were collected through specific analysis of the respective well and used to calculate the Response value using the following formula [21]:

$$\text{Response (\%)} = 100 \times ([RGB]_{sample} - [RGB]_{mean})/([RGB]_{mean} - [RGB]_{ref}) \quad (1)$$

Where $[RGB]_{sample}$: RGB value obtained for the well holding the sample; $[RGB]_{mean}$: RGB value obtained for the wells without adding NaCl; $[RGB]_{ref}$ = 255. The obtained Response values were plotted in a linear regression model against $\log_{10}$[BSA] present in each well, yielding the following equation [21]:

$$\text{Response (\%)} = m \log[BSA] + b \quad (2)$$

Where m: slope of the linear regression curve; b: y-intercept of the obtained linear regression curve. Additionally, the limit of detection (LOD) was also calculated from the following formula [21]:

$$LOD = 3.3 \times(\sigma/m) \quad (3)$$

Where: σ is the standard deviation of the response and m: slope of the linear regression curve obtained from the previous equation.

3. Optical Properties of Metallic NPs

3.1. AuNPs Synthesis and Characterization

Citrate-capped gold nanoparticles (AuNPs) were synthesised following a well-reported Turkevich method [22]. The obtention of a deep-red characteristic colouration in the reactional mixture indicated a well-achieved AuNPs solution. The obtained nanoparticles were first characterised by UV-Vis spectroscopy and DLS analysis, summarising the results in **Figure 1**. AuNPs present a well-defined absorption profile consistent with those reported in the literature for spherical AuNPs, with a typical plasmonic band appearing at 523 nm. Their hydrodynamic diameter (HD) was 32.5 ± 0.3 nm, with a polydispersity index (PDI) of 0.556 ± 0.002. The obtained zeta-potential (ζ) was -30.2 ± 0.7 mV, confirming the successful citrate capping of the particles. TEM was also performed to verify the dispersity, size and morphology of the synthesized nanoparticles. The obtained nanoparticles present a well-defined spherical shape with an average diameter of 14 ± 2 nm. These values are in accordance with others reported in the literature for similar particles [22].

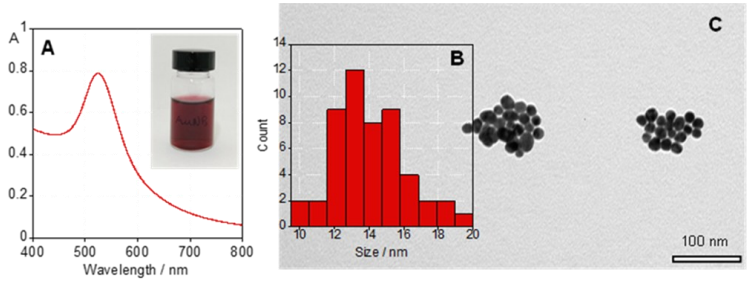

D

	Particle Diameter (nm) TEM	HD (nm)	PDI	Zeta Potential (mV)
AuNPs	14 ± 2	32.5 ± 0.3	0.556 ± 0.002	-30.2 ± 0.7

Figure 1. Characterisation of AuNPs: (A) absorption spectra; inset: colourimetric evaluation of the freshly synthesised AuNPs; (B) Size distribution for nanoparticles from TEM analysis; (C) TEM image; and (D) size and particle surface charge of the synthesised nanoparticles.

3.2. AuNPs-Protein Interaction in Aqueous Environments

To evaluate any interactions that might occur between the nanoparticles and protein, AuNPs were diluted with a dilution factor of 0.18 to a total volume of 2 mL, yielding a homogeneous deep-red nanoparticle suspension. Subsequently, 10 µL of a 2 mg/mL BSA aqueous solution was added to the solution. BSA was selected as a model protein, as albumin is the most prevalent protein in physiological contexts, and the bovine counterpart has similar characteristics to that of the human one. Upon addition of the protein, no colorimetric alterations were verified; however, after the addition of 1 mL of a 5 M NaCl aqueous solution, a substantial colorimetric alteration occurred from red to purple, as seen in **Figure 2**. Upon the addition of NaCl, in the absence of BSA, the nanoparticles lost their deep-red colouration, turning into a clear/grey solution. At each stage, the absorption spectra were collected, and other properties were analysed through DLS, as summarised in **Figure 2**. BSA was added to the AuNPs suspension to a final concentration of 10 µg/mL in the cell. Despite this addition, no colorimetric alterations were observed, with the suspension maintaining its characteristic red colouration. However, from analysis of the UV-Vis spectra, a slight alteration of the absorption maximum was observed, with a shift occurring from 523 to 526 nm. This slight redshift is consistent with reports in the literature regarding protein-AuNPs interaction, possibly through the formation of a "protein corona" [23]. A slight alteration in the hydrodynamic diameter obtained for the AuNPs in the presence and absence of BSA was also verified. This alteration can be derived from forming a "soft corona", meaning the formation of a dynamic layer of protein at the surface of the nanoparticles.

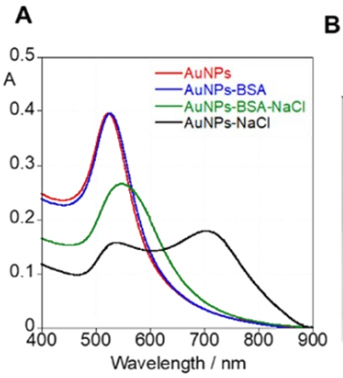

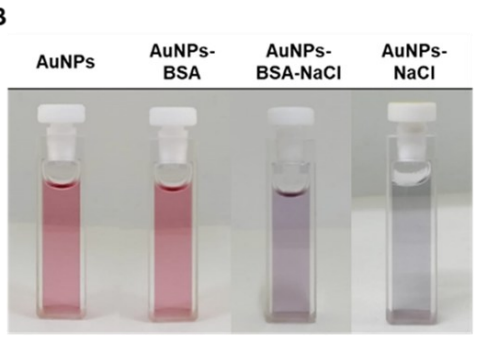

C

	HD (nm)	PDI	Zeta potential (ζ) (mV)
AuNPs	32.5 ± 0.3	0.556 ± 0.002	-30 ± 1
AuNPs-BSA	33.4 ± 0.2	0.542 ± 0.003	-21 ± 1
AuNPs-BSA-NaCl	276 ± 29	0.198 ± 0.008	55 ± 22
AuNPs-NaCl	538 ± 27	0.24 ± 0.03	-3.8 ± 0.4

Figure 2. (A) Absorption spectra of free AuNPs (red); AuNPs in the presence of BSA (blue); AuNPs in the presence of BSA and NaCl (green); AuNPs in the presence of NaCl (black). (B) Colourimetric alterations of the tested conditions; (C) Hydrodynamic diameter, polydispersity index and zeta potential of AuNPs in response to the different tested conditions.

This interaction is, however, clearly noticeable from the zeta-potential data obtained for both solutions. Without the addition of BSA, the AuNPs presented a surface charge of ca. -30 mV, a typical charge for citrate-capped AuNPs, due to the negative charge of the citrate moiety [24]. However, upon BSA addition, this charge was altered to ca. -21 mV. This alteration is indicative of BSA-AuNPs surface interactions, partially neutralising the inherent negative surface charge of the nanoparticles. Interestingly, when adding 1 mL of an aqueous solution of NaCl 5 M, drastically increasing the ionic strength of the solution, a colorimetric alteration took place, changing from red to purple hue. Once again, this alteration was accompanied by a visible alteration in the absorption spectra, where the maximum peak suffered a redshift to 547 nm and a decrease in the absorbance intensity, followed by an increase in the hydrodynamic diameter from 33 nm to 276 nm. Such high values indicate aggregation or clustering phenomena in solution, modulated by the increased ionic strength induced by adding NaCl. Moreover, the zeta-potential measurements indicate a very pronounced charge alteration from the negative values obtained without NaCl. This drastic shift from negative to positive occuring in response to the increased ionic strength of the solution. Several mechanisms might be responsible, however, considering the hydrodynamic diameter values obtained, aggregation phenomena are the most likely to occur. However, another explanation might involve the compression of the electric double layer [25]. This compression could reduce the negative charge available at the surface of the particles, leading to a charge reversal. This effect might also become more pronounced if the free ions in solution adsorb preferentially to the protein corona, particularly Na^+ ions, resulting in a more positive zeta potential.

To best understand the role of NaCl and BSA in these systems, measurements were performed in the same conditions as before, replacing the BSA solution with water. The nanoparticles lost their red colour upon the addition of NaCl, acquiring a clear aspect, with no trace of the purple hue observed in the presence of BSA. Once again, this alteration was accompanied by alterations in the UV-Vis spectra, consistent with other spectra reported in the literature for AuNPs in the presence of increasing NaCl concentrations [24]. Once again, a drastic increase in hydrodynamic diameter was observed, surpassing the values observed for the AuNPs in the presence of BSA and NaCl. These results are once again indicative of the occurrence of aggregation phenomena. Comparing the hydrodynamic diameter measurements obtained for AuNPs-NaCl in the presence and absence of BSA underscores the role of BSA in the AuNPs stabilisation in solution. The presence of BSA appears to help the nanoparticle's stabilisation in the presence of higher ionic strength, although some aggregation persists. Additionally, considering the zeta-potential values obtained for the AuNP-NaCl condition of ca. -3.8 mV, being less negative than those presented by the AuNPs alone but not as positive as the system in the presence of BSA (ca. 55 mV). These differing values might arise due to the absence of a protein corona. As no protein corona exists, fewer Na^+ ions can interact with the negatively charged citrate molecules present on the surface of the particle, thereby neutralizing part of the surface charges available. Under these conditions, the ratio between Na^+ ions and citrate molecules was approximately even, as almost all charges were neutralized. The slight negative charge remaining most likely originates from the citrate molecules that did not interact with the sodium ions in solution.

3.3. High-Throughput Colorimetric Protein Detection in H_2O

Following the above-described assays, the method was scaled down and further optimized for a high-throughput analysis in ultrapure water. Using a 96-well plate as a high-throughput platform, four conditions were prepared, as seen in **Figure 3**. The four conditions tested yielded a clear differential colorimetric profile. Condition 1 combined the AuNPs in a constant concentration with increasing [BSA] ranging from 0 to 97 µg/mL (0, 1, 2, 5, 10, 25, 50, 97 µg/mL). Additionally, a constant NaCl concentration was added to each of the wells. Condition 2 consists of the AuNPs in the presence of BSA without the addition of NaCl. Condition 3 consists of the AuNPs in the presence of NaCl without adding BSA. Finally, Condition 4 consists of AuNPs in water without BSA or NaCl. Similarly to what was verified and discussed in the previous section, the presence of BSA in solution, in contact with AuNPs, allows for the formation of a protein corona, which cannot be readily identifiable through a naked-eye assessment from the simple addition of protein to the AuNPs, requiring a revealing agent, which for the purposes of this work was NaCl. By increasing the ionic strength of the solutions, the nanoparticles tended to aggregate, losing their optical properties. This aggregation, associated with a loss of colour, is also verified in Condition 3, in which, in the absence of BSA, the solution went from a red/pink colouration, as seen in Conditions 2 and 4, to a transparent/grey colour verified in Condition 3. As seen in Condition 1, upon adding NaCl to the BSA-AuNPs complex, the wells acquired a gradient of colouration, ranging from a grey/purple hue to the expected red/pink, traditional of the AuNPs. With a lower [BSA], the amount of protein interacting with the AuNPs will be smaller, forming a less defined protein corona.

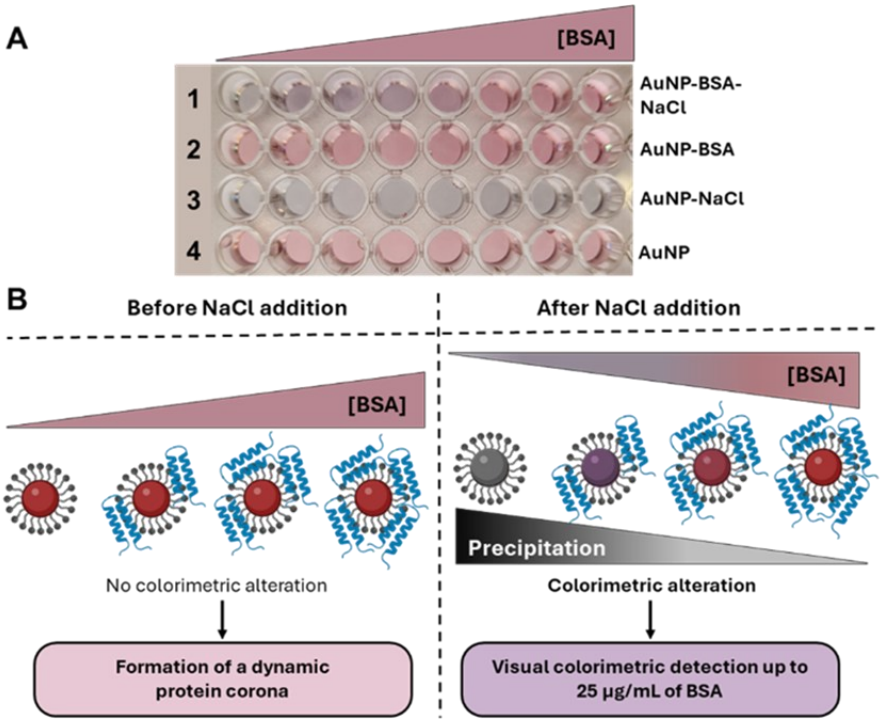

Figure 3. (A) Colourimetric response of AuNPs-BSA solution (with increasing [BSA]), upon NaCl addition in water. (B) Schematic overview of the proposed mechanism of action for AuNP-protein interaction.

With the increase of [BSA], the interactions between protein and nanoparticles will also increase and strengthen the protein corona. Upon the addition of NaCl, the nanoparticles that have the strongest protein corona will not aggregate readily. This precipitation ratio will be inversely proportional to the concentration of BSA in the solution, meaning that the more protein in the solution, the less aggregation and precipitation phenomena will occur. This is also consistent with the observed colorimetric profile. The purple hue appears to be an intermediate state between total aggregation/precipitation and a complete protein corona that protects the nanoparticles and prevents the occurrence of these phenomena.

3.4. AuNPs-Protein Interaction in Human Urine Samples

Following the promising data obtained for scaling down the assay in water, the same methodology was applied to urine samples to assess the method's applicability for protein detection in biological samples. Six different urine samples were collected from healthy volunteers (n = 6; 50% male and 50% female). To ensure sample and biological diversity, the urines were collected from healthy individuals with different hydration levels on the same day. The urine samples were first subjected to a simple paper filtration to remove any solid deposits and then diluted in H_2O to a 1:20 ratio. Each diluted urine sample was then spiked with specific volumes of BSA to ensure a protein gradient of 0 to 97 µg/mL. Following this, 170 µL of each spiked urine solution was added to a 96-well plate, followed by the subsequent addition of 30 µL of AuNPs and 20 µL of a 5M NaCl aqueous solution. The same colorimetric gradient was observed, consistent with the results obtained in the water-based assay as seen in **Figure 4**. The solution's colouration shifted from a grey/purple hue to a red/pink hue as the BSA concentration in the solution grew. The BSA concentration range in urine was like the one tested in water, displaying a similar colorimetric behaviour across different samples. To verify the consistency of the assay, various urine samples were evaluated through this method, resulting in colour changes like those observed in water. The first five wells, corresponding to a BSA concentration of 0-10 µg/mL, exhibited a purple/grey hue, while wells from the sixth onward remained with the red/pink hue upon NaCl addition. This consistency obtained between the various samples aligns with the proposed mechanism in which, with the increase of BSA in solution, a more stable protein corona forms around the particles, decreasing the precipitation/aggregation phenomena that could occur upon the increase of ionic strength modulated *via* NaCl addition. A similar procedure was performed with the human urine of a patient with colorectal cancer without the addition of BSA. The total protein quantity in the sample was also quantified using Bradford assay.

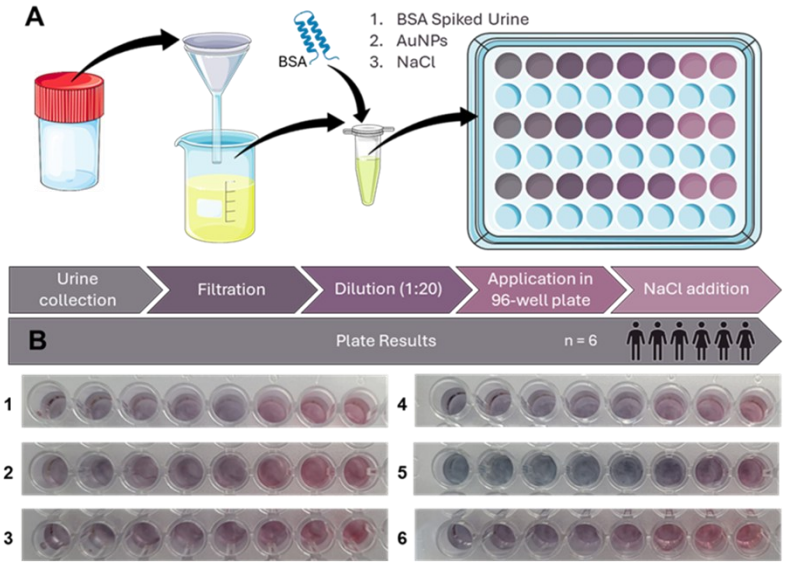

Figure 4. (A) Schematic overview of the urine analysis process, from urine collection and treatment to plate application. (B) Colorimetric response of AuNPs-BSA solution (with increasing [BSA]), upon NaCl addition in urine.

3.5. RGB Smartphone-Assisted Analysis for Protein Quantification

As the method described above allowed for a qualitative determination of protein in solution through a colorimetric alteration, we aimed to develop a quantitative approach for protein quantification in solution, using AuNPs as colorimetric indicators. This approach was based on others already published in the literature, where, through RGB analysis of a photograph, it is possible to quantify a specific analyte that triggers a colorimetric response on the indicator [21,26,27]. To verify if such an approach was feasible, the first step was to confirm if a linear correlation between the RGB response and the respective BSA concentration in the solution could be obtained. To this end, a BSA gradient in water was performed with the following concentrations: 0, 1, 2, 5, 10, 25, 50, 97 µg/mL, in the presence and absence of NaCl, like the above-mentioned assays in water. Images of the plates were captured with a Samsung Galaxy S21 FE 5G smartphone positioned ca. 20 cm above the plate. The plates were photographed under natural light, without direct sunlight irradiation, to prevent reflectance

interference in the 96-well plate. The captured images were then analysed using the free, open-source ImageJ Software [28] to conduct an RGB analysis. A comprehensive colorimetric analysis was performed, obtaining the respective RGB means, as well as the individual Red, Blue and Green Channels for each well. A selection of 5000 pixels, circular area measurement in ImageJ, was performed in the center part of the wells and all subsequent measurements and colorimetric information was derived from this selection. From here, following a similar approach already reported in the literature, the Response % (R%) was calculated using **Equation 1**, as illustrated in **Figure 5**.

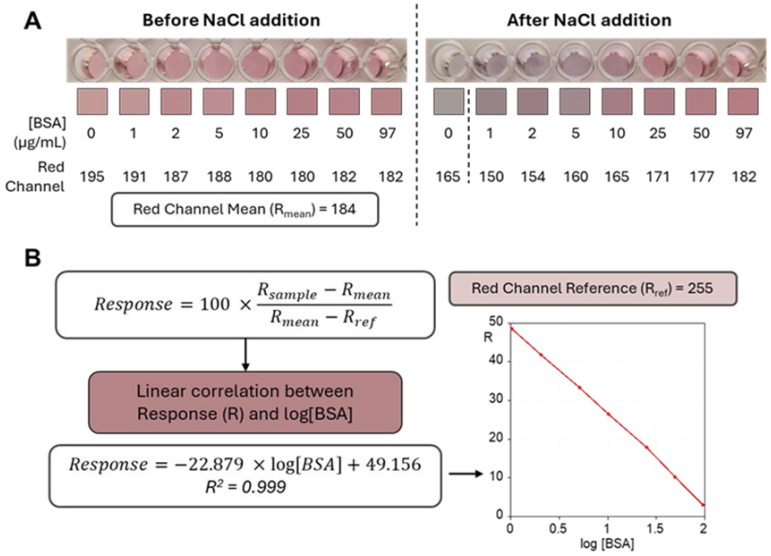

Figure 5. (A) Colorimetric analysis of the water-based calibration curve. (B) Mathematical deduction for Response % calculation and linear correlation between Response % and log [BSA].

This percentage was calculated for all the obtained variations of the RGB analysis: RGB mean, Red Channel mean, Blue Channel mean, and Green Channel mean. The analysis demonstrated that the Red Channel values exhibited the most reliable results, demonstrating a strong linear correlation with protein concentration in solution. In contrast, the blue and green channels had a lower variation in response to the protein gradient and were discarded from further analysis. From here, all further studies were conducted exclusively using the Red Channel mean values. **Figure 5** shows the images obtained, their colorimetric analysis, and their respective mathematical approaches. Using the Red Channel mean values it is possible to calculate the Response (%) and correlate it with the log [BSA] values. A strong linear correlation between these two variables was obtained, demonstrating the feasibility of protein quantification through this method. Moreover, the Limit of Detection (LOD) was also calculated [21] from this dataset, being 1.19 µg/mL, with respect to BSA concentration, a value comparable to other protein quantification methods, as seen in **Table SN1**. From here, we moved on to the evaluation of biological samples under the same conditions as described in the above sections, with respect to the assays involving urine samples. Once again, a constant BSA concentration gradient was maintained in the samples. Plate images were captured with three different smartphone models (Samsung Galaxy S21 FE 5G, OPPO Reno 8 Lite and iPhone 14 Pro) to introduce variation in the analysis and assess the consistency of the method across different camera and smartphone models. Once again, the images were obtained under natural light without direct sun irradiation to avoid the occurrence of reflections in the photograph, at ca. 20 cm from the plate.

The images obtained were evaluated using the ImageJ software, with mean Red Channel values obtained for each condition. After this colorimetric analysis, the recovery percentage was calculated to assess the accuracy of each smartphone model. Additionally, an ANOVA statistical analysis (n = 6; α = 0.05) was performed to evaluate the potential statistical variance within each smartphone model. The results, as shown in **Table SN2**, indicate that for all models, the p-values were greater than 0.05, suggesting no significant variation in recovery percentages among the individual measurements for each smartphone model. **Table 1** summarises the results obtained for each smartphone model tested. All p-values were $p > 0.05$. The complete recovery data for all BSA concentrations and respective Recovery % values are included in the Supplementary Material. From the previous table's analysis, it becomes clear that the Recovery (%) values were close to 100%, demonstrating the assay's reliability in estimating a quantitative determination of protein in urine in the proposed conditions. Moreover, the statistical ANOVA analysis also demonstrates no significant differences between the smartphone models used, proposing that this method might be used regardless of the smartphone model and camera characteristics used. In addition to these analysis and validation tests, a similar approach was conducted using a urine sample from a patient with colorectal cancer as a preliminary proof of concept for the implementation of this methodology in clinically relevant samples. This sample underwent a parallel assessment through the Bradford assay to allow for a comparative analysis between one of the most employed and established protein quantification methods and the proposed colorimetric method.

Table 1. Summary of the Response % obtained for each smartphone model.

Smartphone model	Individual	%Recovery ± Standard Deviation
Samsung Galaxy S21 FE 5G	1	111 ± 12
	2	105 ± 14
	3	108 ± 6
	4	125 ± 12
	5	105 ± 17
	6	111 ± 11
iPhone 14 Pro	1	95 ± 10
	2	113 ± 14
	3	112 ± 11
	4	113 ± 15
	5	115 ± 15
	6	109 ± 10
OPPO Reno 8 Lite	1	104 ± 9
	2	104 ± 14
	3	114 ± 7
	4	109 ± 10
	5	110 ± 13
	6	99 ± 9

Figure 6 summarises the protein quantification results obtained from the two methods. The image was analysed using the ImageJ software, analysing the section highlighted in **Figure 6**.

From these data, we obtained a Response % of 44.59, which translates to a protein concentration of ca. 1.8 ± 0.2 µg/mL. Considering the dilution factors, the protein concentration in the urine sample calculated through our method was 37 ± 3 µg/mL. In comparison, Bradford quantification yielded a total protein concentration of ca. 41 ± 1 µg/mL. These two values are similar to each other, allowing for the validation of this assay as a powerful tool for protein quantification in urine through a simple, fast and high-throughput method, which relies on a simple photograph analysis obtained *via* a smartphone camera.

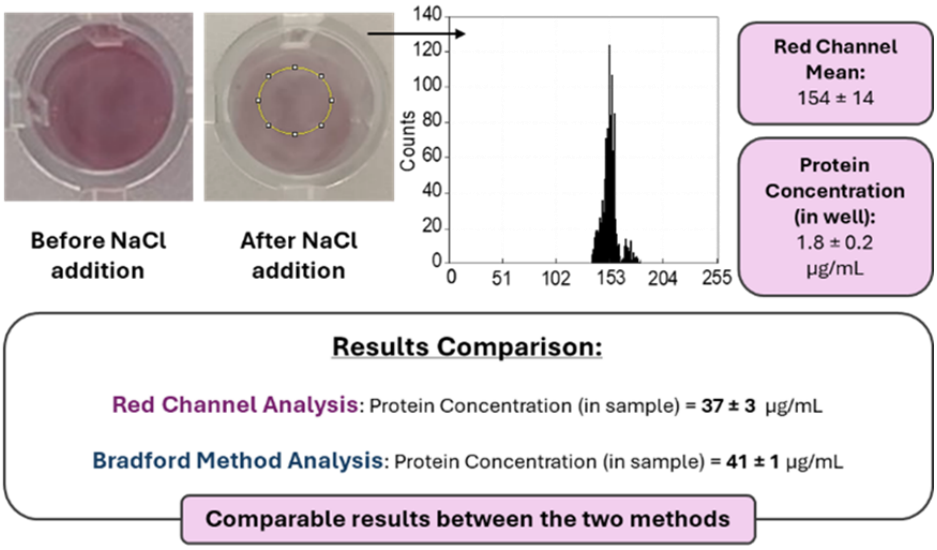

Figure 6. Summary of the colorimetric analysis of the patient's urine and respective protein quantification results obtained from the Red Channel Analysis and Bradford Method Analysis.

5. Concluding Remarks

In this study, we have demonstrated the feasibility of using gold nanoparticles (AuNPs) for sensitive and specific protein detection, mainly albumin, in urine samples. The interaction between AuNPs and proteins, facilitated by NaCl, induced distinct colorimetric changes that were quantitatively analysed using RGB values obtained from smartphone images. This method showed promising results in visually detecting protein concentrations as low as 25 µg/mL in both aqueous solutions and urine samples. Integrating smartphone-based RGB analysis further enhances the method's accessibility and usability, enabling the determination of protein with a detection limit of 1.19 µg/mL. Moreover, the assay results were also effective for monitoring protein in CRC, where a protein concentration value of 37.17 µg/mL was determined and further validated by the Bradford method. This approach shows great potential for the early detection and monitoring of urinary protein through non-invasive analysis. By offering a rapid, cost-effective, and portable method for protein quantification, our findings may offer a useful tool for monitoring proteinuria in patients.

Supplementary Material

The following supplementary material is available: **Table SN1**: Limits of Detection (LOD) for various techniques for protein detection and quantification; **Table SN2**: Response% data obtained for each smartphone model and each specific condition.

Acknowledgements

This work was financed by national funds from FCT - Fundação para a Ciência e a Tecnologia, I.P., under the scope of the project UID/50006/2023 of the Associate Laboratory for Green Chemistry-LAQV REQUIMTE; as well as the PROTEOMASS Scientific Society (Portugal) for funding support (General Funding Grant 2023–2024). J.G. thanks FCT/MCTES for doctoral support (Grant 2022.09495.BD; https://doi.org/10.54499/2022.09495.BD). E.O. thanks Universidade Nova de Lisboa and Fundação para a Ciência e a Tecnologia (FCT) for the Assistant Professor contract granted under the FCT Tenure Programme (2023.11076.TENURE.116). H.M.S. thanks LAQV for his research contract support. We extend our sincere gratitude to Professors C. Lodeiro and J.L. Capelo for their invaluable contributions, particularly in securing funding for state-of-the-art instrumentation at NOVA FCT through collaborative efforts, which have been essential for the success of this research.

Informed Consent Statement

Informed consent was obtained from all subjects involved in the study.

References

[1] K. Tryggvason, E. Pettersson, Causes and consequences of proteinuria: the kidney filtration barrier and progressive renal failure, J Intern Med 254 (2003) 216–224. https://doi.org/10.1046/J.1365-2796.2003.01207.X.

[2] J. Park, D.W. Shin, K. Han, D. Kim, S. Chun, H.R. Jang, Associations Between Kidney Function, Proteinuria, and the Risk of Kidney Cancer: A Nationwide Cohort Study Involving 10 Million Participants, Am J Epidemiol 190 (2021) 2042–2052. https://doi.org/10.1093/aje/kwab140.

[3] S. Aitekenov, A. Gaipov, R. Bukasov, Review: Detection and quantification of proteins in human urine, Talanta 223 (2021) 121718. https://doi.org/10.1016/j.talanta.2020.121718.

[4] A.S.A. Naderi, R.F. Reilly, Primary Care Approach to Proteinuria, The Journal of the American Board of Family Medicine 21 (2008) 569–574. https://doi.org/10.3122/jabfm.2008.06.070080.

[5] J.E. Toblli, P. Bevione, F. Di Gennaro, L. Madalena, G. Cao, M. Angerosa, Understanding the Mechanisms of Proteinuria: Therapeutic Implications, Int J Nephrol 2012 (2012) 1–13. https://doi.org/10.1155/2012/546039.

[6] D. Lim, D.-Y. Lee, S.H. Cho, O.Z. Kim, S.W. Cho, S.K. An, H.W. Kim, K.H. Moon, M.H. Lee, B. Kim, Diagnostic accuracy of urine dipstick for proteinuria in older outpatients, Kidney Res Clin Pract 33 (2014) 199–203. https://doi.org/10.1016/j.krcp.2014.10.003.

[7] J.G. Song, K.C. Baral, G.-L. Kim, J.-W. Park, S.-H. Seo, D.-H. Kim, D.H. Jung, N.L. Ifekpolugo, H.-K. Han, Quantitative analysis of therapeutic proteins in biological fluids: recent advancement in analytical techniques, Drug Deliv 30 (2023). https://doi.org/10.1080/10717544.2023.2183816.

[8] F. Jia, Q. Liu, W. Wei, Z. Chen, Colorimetric sensor assay for discrimination of proteins based on exonuclease I-triggered aggregation of DNA-functionalized gold nanoparticles, Analyst 144 (2019) 4865–4870. https://doi.org/10.1039/C9AN00918C.

[9] L. Treuel, G.U. Nienhaus, Toward a molecular understanding of nanoparticle–protein interactions, Biophys Rev 4 (2012) 137–147. https://doi.org/10.1007/s12551-012-0072-0.

[10] P. Breznica, R. Koliqi, A. Daka, A review of the current understanding of nanoparticles protein corona composition, Med Pharm Rep 93 (2020) 342–350. https://doi.org/10.15386/mpr-1756.

[11] S.R. Saptarshi, A. Duschl, A.L. Lopata, Interaction of nanoparticles with proteins: relation to bio-reactivity of the nanoparticle, J Nanobiotechnology 11 (2013) 26. https://doi.org/10.1186/1477-3155-11-26.

[12] G. Bashiri, M.S. Padilla, K.L. Swingle, S.J. Shepherd, M.J. Mitchell, K. Wang, Nanoparticle protein corona: from structure and function to therapeutic targeting, Lab Chip 23 (2023) 1432–1466. https://doi.org/10.1039/D2LC00799A.

[13] Y.T. Ho, B. Poinard, E.L.L. Yeo, J.C.Y. Kah, An instantaneous colorimetric protein assay based on spontaneous formation of a protein corona on gold nanoparticles, Analyst 140 (2015) 1026–1036. https://doi.org/10.1039/C4AN01819B.

[14] S.H. Elagamy, L. Adly, M.A. Abdel Hamid, Smartphone based colorimetric approach for quantitative determination of uric acid using Image J, Scientific Reports 2023 13:1 13 (2023) 1–9. https://doi.org/10.1038/s41598-023-48962-0.

[15] R. Sivakumar, N.Y. Lee, Recent progress in smartphone-based techniques for food safety and the detection of heavy metal ions in environmental water, Chemosphere 275 (2021) 130096. https://doi.org/10.1016/J.CHEMOSPHERE.2021.130096.

[16] T. Zhao, X. Liang, X. Guo, X. Yang, J. Guo, X. Zhou, X. Huang, W. Zhang, Y. Wang, Z. Liu, Z. Jiang, H. Zhou, H. Zhou, Smartphone-based colorimetric sensor array using gold nanoparticles for rapid distinguishment of multiple pesticides in real samples, Food Chem 404 (2023) 134768. https://doi.org/10.1016/J.FOODCHEM.2022.134768.

[17] F.J. Cao, H.H. Cheng, S.X. Ma, F. Jiao, D.M. Dong, Three-channel smartphone-based aptamer sensor for multiplexed detecting antibiotics in water through resonance light scattering, Sens Biosensing Res 38 (2022) 100533. https://doi.org/10.1016/J.SBSR.2022.100533.

[18] B. Peng, J. Zhou, J. Xu, M. Fan, Y. Ma, M. Zhou, T. Li, S. Zhao, A smartphone-based colorimetry after dispersive liquid–liquid microextraction for rapid quantification of calcium in water and food samples, Microchemical Journal 149 (2019) 104072. https://doi.org/10.1016/J.MICROC.2019.104072.

[19] J. Turkevich, P.C. Stevenson, J. Hillier, A study of the nucleation and growth processes in the synthesis of colloidal gold, Discuss Faraday Soc 11 (1951) 55. https://doi.org/10.1039/df9511100055.

[20] M.M. Bradford, A rapid and sensitive method for the quantitation of microgram quantities of protein utilizing the principle of protein-dye binding, Anal Biochem 72 (1976) 248–254. https://doi.org/10.1016/0003-2697(76)90527-3.

[21] E. Tan, İ.M. Kahyaoğlu, S. Karakuş, A sensitive and smartphone colorimetric assay for the detection of hydrogen peroxide based on antibacterial and antifungal matcha extract silver nanoparticles enriched with polyphenol, Polymer Bulletin 79 (2022) 7363–7389. https://doi.org/10.1007/s00289-021-03857-w.

[22] G.A. Marcelo, M.P. Duarte, E. Oliveira, Gold@mesoporous silica nanocarriers for the effective delivery of antibiotics and by-passing of β-lactam resistance, SN Appl Sci 2 (2020) 1354. https://doi.org/10.1007/s42452-020-3023-6.

[23] A. Gomes, J.M. Carnerero, A. Jimenez-Ruiz, E. Grueso, R.M. Giráldez-Pérez, R. Prado-Gotor, Lysozyme–AuNPs Interactions: Determination of Binding Free Energy, Nanomaterials 11 (2021) 2139. https://doi.org/10.3390/nano11082139.

[24] S. Vijayakumar, S. Ganesan, Preparation and stability of gold nanoparticles, Indian Journal of Physics 86 (2012) 989–995. https://doi.org/10.1007/s12648-012-0161-8.

[25] S. Bhattacharjee, DLS and zeta potential – What they are and what they are not?, Journal of Controlled Release 235 (2016) 337–351. https://doi.org/10.1016/j.jconrel.2016.06.017.

[26] G. de Carvalho Oliveira, C.C.S. Machado, D.K. Inácio, J.F. da Silveira Petruci, S.G. Silva, RGB color sensor for colorimetric determinations: Evaluation and quantitative analysis of colored liquid samples, Talanta 241 (2022) 123244. https://doi.org/10.1016/j.talanta.2022.123244.

[27] L. Engel, I. Benito-Altamirano, K.R. Tarantik, C. Pannek, M. Dold, J.D. Prades, J. Wöllenstein, Printed sensor labels for colorimetric detection of ammonia, formaldehyde and hydrogen sulfide from the ambient air, Sens Actuators B Chem 330 (2021) 129281. https://doi.org/10.1016/j.snb.2020.129281.

[28] C.A. Schneider, W.S. Rasband, K.W. Eliceiri, NIH Image to ImageJ: 25 years of image analysis, Nat Methods 9 (2012) 671–675. https://doi.org/10.1038/nmeth.2089.